

Measurement of single electrons and implications for charm production in Au+Au collisions at $\sqrt{s_{NN}} = 130$ GeV

K. Adcox,⁴⁰ S. S. Adler,³ N. N. Ajitanand,²⁷ Y. Akiba,¹⁴ J. Alexander,²⁷ L. Aphecetche,³⁴ Y. Arai,¹⁴ S. H. Aronson,³ R. Averbeck,²⁸ T. C. Awes,²⁹ K. N. Barish,⁵ P. D. Barnes,¹⁹ J. Barrette,²¹ B. Bassalleck,²⁵ S. Bathe,²² V. Baublis,³⁰ A. Bazilevsky,^{12,32} S. Belikov,^{12,13} F. G. Bellaiche,²⁹ S. T. Belyaev,¹⁶ M. J. Bennett,¹⁹ Y. Berdnikov,³⁵ S. Botelho,³³ M. L. Brooks,¹⁹ D. S. Brown,²⁶ N. Bruner,²⁵ D. Bucher,²² H. Buesching,²² V. Bumazhnov,¹² G. Bunce,^{3,32} J. Burward-Hoy,²⁸ S. Butsyk,^{28,30} T. A. Carey,¹⁹ P. Chand,² J. Chang,⁵ W. C. Chang,¹ L. L. Chavez,²⁵ S. Chernichenko,¹² C. Y. Chi,⁸ J. Chiba,¹⁴ M. Chiu,⁸ R. K. Choudhury,² T. Christ,²⁸ T. Chujo,^{3,39} M. S. Chung,^{15,19} P. Chung,²⁷ V. Cianciolo,²⁹ B. A. Cole,⁸ D. G. D'Enterria,³⁴ G. David,³ H. Delagrange,³⁴ A. Denisov,¹² A. Deshpande,³² E. J. Desmond,³ O. Dietzsch,³³ B. V. Dinesh,² A. Drees,²⁸ A. Durum,¹² D. Dutta,² K. Ebisu,²⁴ Y. V. Efremenko,²⁹ K. El Chenawi,⁴⁰ H. En'yo,^{17,31} S. Esumi,³⁹ L. Ewell,³ T. Ferdousi,⁵ D. E. Fields,²⁵ S. L. Fokin,¹⁶ Z. Fraenkel,⁴² A. Franz,³ A. D. Frawley,⁹ S.-Y. Fung,⁵ S. Garpman,^{20,*} T. K. Ghosh,⁴⁰ A. Glenn,³⁶ A. L. Godoi,³³ Y. Goto,³² S. V. Greene,⁴⁰ M. Grosse Perdekamp,³² S. K. Gupta,² W. Guryn,³ H. -Å. Gustafsson,²⁰ T. Hachiya,¹¹ J. S. Haggerty,³ H. Hamagaki,⁷ A. G. Hansen,¹⁹ H. Hara,²⁴ E. P. Hartouni,¹⁸ R. Hayano,³⁸ N. Hayashi,³¹ X. He,¹⁰ T. K. Hemmick,²⁸ J. M. Heuser,²⁸ M. Hibino,⁴¹ J. C. Hill,¹³ D. S. Ho,⁴³ K. Homma,¹¹ B. Hong,¹⁵ A. Hoover,²⁶ T. Ichihara,^{31,32} K. Imai,^{17,31} M. S. Ippolitov,¹⁶ M. Ishihara,^{31,32} B. V. Jacak,^{28,32} W. Y. Jang,¹⁵ J. Jia,²⁸ B. M. Johnson,³ S. C. Johnson,^{18,28} K. S. Joo,²³ S. Kametani,⁴¹ J. H. Kang,⁴³ M. Kann,³⁰ S. S. Kapoor,² S. Kelly,⁸ B. Khachaturov,⁴² A. Khanzadeev,³⁰ J. Kikuchi,⁴¹ D. J. Kim,⁴³ H. J. Kim,⁴³ S. Y. Kim,⁴³ Y. G. Kim,⁴³ W. W. Kinnison,¹⁹ E. Kistenev,³ A. Kiyomichi,³⁹ C. Klein-Boesing,²² S. Klinksiek,²⁵ L. Kochenda,³⁰ V. Kochetkov,¹² D. Koehler,²⁵ T. Kohama,¹¹ D. Kotchetkov,⁵ A. Kozlov,⁴² P. J. Kroon,³ K. Kurita,^{31,32} M. J. Kweon,¹⁵ Y. Kwon,⁴³ G. S. Kyle,²⁶ R. Lacey,²⁷ J. G. Lajoie,¹³ J. Lauret,²⁷ A. Lebedev,^{13,16} D. M. Lee,¹⁹ M. J. Leitch,¹⁹ X. H. Li,⁵ Z. Li,^{6,31} D. J. Lim,⁴³ M. X. Liu,¹⁹ X. Liu,⁶ Z. Liu,⁶ C. F. Maguire,⁴⁰ J. Mahon,³ Y. I. Makdisi,³ V. I. Manko,¹⁶ Y. Mao,^{6,31} S. K. Mark,²¹ S. Markacs,⁸ G. Martinez,³⁴ M. D. Marx,²⁸ A. Masaike,¹⁷ F. Matathias,²⁸ T. Matsumoto,^{7,41} P. L. McGaughey,¹⁹ E. Melnikov,¹² M. Merschmeyer,²² F. Messer,²⁸ M. Messer,³ Y. Miake,³⁹ T. E. Miller,⁴⁰ A. Milov,⁴² S. Mioduszewski,^{3,36} R. E. Mischke,¹⁹ G. C. Mishra,¹⁰ J. T. Mitchell,³ A. K. Mohanty,² D. P. Morrison,³ J. M. Moss,¹⁹ F. Mühlbacher,²⁸ M. Muniruzzaman,⁵ J. Murata,³¹ S. Nagamiya,¹⁴ Y. Nagasaka,²⁴ J. L. Nagle,⁸ Y. Nakada,¹⁷ B. K. Nandi,⁵ J. Newby,³⁶ L. Nikkinen,²¹ P. Nilsson,²⁰ S. Nishimura,⁷ A. S. Nyanin,¹⁶ J. Nystrand,²⁰ E. O'Brien,³ C. A. Ogilvie,¹³ H. Ohnishi,^{3,11} I. D. Ojha,^{4,40} M. Ono,³⁹ V. Onuchin,¹² A. Oskarsson,²⁰ L. Österman,²⁰ I. Otterlund,²⁰ K. Oyama,^{7,38} L. Paffrath,^{3,*} A. P. T. Palounek,¹⁹ V. S. Pantuev,²⁸ V. Papavassiliou,²⁶ S. F. Pate,²⁶ T. Peitzmann,²² A. N. Petridis,¹³ C. Pinkenburg,^{3,27} R. P. Pisani,³ P. Pitukhin,¹² F. Plasil,²⁹ M. Pollack,^{28,36} K. Pope,³⁶ M. L. Purschke,³ I. Ravinovich,⁴² K. F. Read,^{29,36} K. Reygers,²² V. Riabov,^{30,35} Y. Riabov,³⁰ M. Rosati,¹³ A. A. Rose,⁴⁰ S. S. Ryu,⁴³ N. Saito,^{31,32} A. Sakaguchi,¹¹ T. Sakaguchi,^{7,41} H. Sako,³⁹ T. Sakuma,^{31,37} V. Samsonov,³⁰ T. C. Sangster,¹⁸ R. Santo,²² H. D. Sato,^{17,31} S. Sato,³⁹ S. Sawada,¹⁴ B. R. Schleier,¹⁹ Y. Schutz,³⁴ V. Semenov,¹² R. Seto,⁵ T. K. Shea,³ I. Shein,¹² T. -A. Shibata,^{31,37} K. Shigaki,¹⁴ T. Shiina,¹⁹ Y. H. Shin,⁴³ I. G. Sibiriak,¹⁶ D. Silvermyr,²⁰ K. S. Sim,¹⁵ J. Simon-Gillo,¹⁹ C. P. Singh,⁴ V. Singh,⁴ M. Sivertz,³ A. Soldatov,¹² R. A. Soltz,¹⁸ S. Sorensen,^{29,36} P. W. Stankus,²⁹ N. Starinsky,²¹ P. Steinberg,⁸ E. Stenlund,²⁰ A. Ster,⁴⁴ S. P. Stoll,³ M. Sugioka,^{31,37} T. Sugitate,¹¹ J. P. Sullivan,¹⁹ Y. Sumi,¹¹ Z. Sun,⁶ M. Suzuki,³⁹ E. M. Takagui,³³ A. Taketani,³¹ M. Tamai,⁴¹ K. H. Tanaka,¹⁴ Y. Tanaka,²⁴ E. Taniguchi,^{31,37} M. J. Tannenbaum,³ J. Thomas,²⁸ J. H. Thomas,¹⁸ T. L. Thomas,²⁵ W. Tian,^{6,36} J. Tojo,^{17,31} H. Torii,^{17,31} R. S. Towell,¹⁹ I. Tserruya,⁴² H. Tsuruoka,³⁹ A. A. Tsvetkov,¹⁶ S. K. Tuli,⁴ H. Tydesjö,²⁰ N. Tyurin,¹² T. Ushiroda,²⁴ H. W. van Hecke,¹⁹ C. Velissaris,²⁶ J. Velkovska,²⁸ M. Velkovsky,²⁸ A. A. Vinogradov,¹⁶ M. A. Volkov,¹⁶ A. Vorobyov,³⁰ E. Vznuzdaev,³⁰ H. Wang,⁵ Y. Watanabe,^{31,32} S. N. White,³ C. Witzig,³ F. K. Wohn,¹³ C. L. Woody,³ W. Xie,^{5,42} K. Yagi,³⁹ S. Yokkaichi,³¹ G. R. Young,²⁹ I. E. Yushmanov,¹⁶ W. A. Zajc,⁸ Z. Zhang,²⁸ and S. Zhou⁶
(PHENIX Collaboration)

¹ Institute of Physics, Academia Sinica, Taipei 11529, Taiwan² Bhabha Atomic Research Centre, Bombay 400 085, India³ Brookhaven National Laboratory, Upton, NY 11973-5000, USA⁴ Department of Physics, Banaras Hindu University, Varanasi 221005, India⁵ University of California - Riverside, Riverside, CA 92521, USA⁶ China Institute of Atomic Energy (CIAE), Beijing, People's Republic of China⁷ Center for Nuclear Study, Graduate School of Science, University of Tokyo, 7-3-1 Hongo, Bunkyo, Tokyo 113-0033, Japan⁸ Columbia University, New York, NY 10027 and Nevis Laboratories, Irvington, NY 10533, USA⁹ Florida State University, Tallahassee, FL 32306, USA¹⁰ Georgia State University, Atlanta, GA 30303, USA

¹¹*Hiroshima University, Kagamiyama, Higashi-Hiroshima 739-8526, Japan*

¹²*Institute for High Energy Physics (IHEP), Protvino, Russia*

¹³*Iowa State University, Ames, IA 50011, USA*

¹⁴*KEK, High Energy Accelerator Research Organization, Tsukuba-shi, Ibaraki-ken 305-0801, Japan*

¹⁵*Korea University, Seoul, 136-701, Korea*

¹⁶*Russian Research Center "Kurchatov Institute", Moscow, Russia*

¹⁷*Kyoto University, Kyoto 606, Japan*

¹⁸*Lawrence Livermore National Laboratory, Livermore, CA 94550, USA*

¹⁹*Los Alamos National Laboratory, Los Alamos, NM 87545, USA*

²⁰*Department of Physics, Lund University, Box 118, SE-221 00 Lund, Sweden*

²¹*McGill University, Montreal, Quebec H3A 2T8, Canada*

²²*Institut für Kernphysik, University of Münster, D-48149 Münster, Germany*

²³*Myongji University, Yongin, Kyonggido 449-728, Korea*

²⁴*Nagasaki Institute of Applied Science, Nagasaki-shi, Nagasaki 851-0193, Japan*

²⁵*University of New Mexico, Albuquerque, NM 87131, USA*

²⁶*New Mexico State University, Las Cruces, NM 88003, USA*

²⁷*Chemistry Department, State University of New York - Stony Brook, Stony Brook, NY 11794, USA*

²⁸*Department of Physics and Astronomy, State University of New York - Stony Brook, Stony Brook, NY 11794, USA*

²⁹*Oak Ridge National Laboratory, Oak Ridge, TN 37831, USA*

³⁰*PNPI, Petersburg Nuclear Physics Institute, Gatchina, Russia*

³¹*RIKEN (The Institute of Physical and Chemical Research), Wako, Saitama 351-0198, JAPAN*

³²*RIKEN BNL Research Center, Brookhaven National Laboratory, Upton, NY 11973-5000, USA*

³³*Universidade de São Paulo, Instituto de Física, Caixa Postal 66318, São Paulo CEP05315-970, Brazil*

³⁴*SUBATECH (Ecole des Mines de Nantes, IN2P3/CNRS, Université de Nantes) BP 20722 - 44307, Nantes-cedex 3, France*

³⁵*St. Petersburg State Technical University, St. Petersburg, Russia*

³⁶*University of Tennessee, Knoxville, TN 37996, USA*

³⁷*Department of Physics, Tokyo Institute of Technology, Tokyo, 152-8551, Japan*

³⁸*University of Tokyo, Tokyo, Japan*

³⁹*Institute of Physics, University of Tsukuba, Tsukuba, Ibaraki 305, Japan*

⁴⁰*Vanderbilt University, Nashville, TN 37235, USA*

⁴¹*Waseda University, Advanced Research Institute for Science and Engineering, 17 Kikui-cho, Shinjuku-ku, Tokyo 162-0044, Japan*

⁴²*Weizmann Institute, Rehovot 76100, Israel*

⁴³*Yonsei University, IPAP, Seoul 120-749, Korea*

⁴⁴*KFKI Research Institute for Particle and Nuclear Physics (RMKI), Budapest, Hungary[†]*

(May 21, 2019)

Transverse momentum spectra of electrons from Au+Au collisions at $\sqrt{s_{NN}} = 130$ GeV have been measured at midrapidity by the PHENIX experiment at RHIC. The spectra show an excess above the background from photon conversions and light hadron decays. The electron signal is consistent with that expected from semi-leptonic decays of charm. The yield of the electron signal dN_e/dy for $p_T > 0.8$ GeV/c is $0.025 \pm 0.004(\text{stat.}) \pm 0.010(\text{sys.})$ in central collisions, and the corresponding charm cross section is $380 \pm 60(\text{stat.}) \pm 200(\text{sys.}) \mu\text{b}$ per binary nucleon-nucleon collision.

PACS numbers: 25.75.Dw

In this letter, we report the first measurement of single electron spectra, $(e^+ + e^-)/2$, in Au+Au collisions at $\sqrt{s_{NN}} = 130$ GeV by the PHENIX experiment at the Relativistic Heavy Ion Collider (RHIC). The measurement of single leptons at high transverse momentum ($p_T \gtrsim 1$ GeV/c) is a useful way to study heavy-quark production, which is an important probe of hot and dense matter created in high energy heavy ion collisions. Charm production is sensitive to the initial state gluon density [1,2]. Nuclear and medium effects, such as shadowing and charm quark energy loss [3,4], can be studied by comparison of charm production in AA , pA ,

and pp collisions. Measurement of charm is important for understanding J/ψ suppression (a proposed signal of the deconfinement phase transition [5,6]) and the dilepton mass distribution in $1 < M_{l+l^-} < 3$ GeV, where lepton pairs from charm make significant contributions [7]. In pp collisions at the ISR ($\sqrt{s} = 30 - 63$ GeV), production of single electrons was observed ($e/\pi \sim 10^{-4}$) for $p_T > 1$ GeV/c [8–11], and interpreted as evidence of open charm production [12]. In pp collisions at RHIC energies, the signal level is expected to be higher, since charm production increases with $\sqrt{s_{NN}}$ faster than pion production. We recently observed suppression of high p_T

pion production in Au+Au collisions at RHIC relative to binary nucleon-nucleon (NN) collision scaling [13]. If charm production scales with NN collisions, as expected in the absence of nuclear effects, the e/π ratio would be even higher in Au+Au collisions at RHIC.

Data used for this analysis were recorded by the PHENIX west-arm spectrometer [14] ($\Delta\phi = 90^\circ$ in azimuth, $|\eta| < 0.35$ in pseudo-rapidity) during the first RHIC run. The spectrometer consisted of a drift chamber (DC), a layer of pad chambers (PC1), a ring imaging Cerenkov detector (RICH), and a lead-scintillator electromagnetic calorimeter (EMCAL). The trigger was provided by a pair of beam-beam counters (BBC) and a pair of zero-degree calorimeters (ZDC), and covered the most central $92 \pm 4\%$ of Au+Au collisions.

The analysis uses 1.23 M minimum bias events with vertex position $|z| < 30$ cm. Charged particle tracks are reconstructed by the DC and the PC1, and their momenta p are determined by the DC with a resolution of $\delta p/p \simeq 0.6\% \oplus 3.6\% p$ (GeV/c). Tracks are confirmed by a matching hit in the EMCAL, which measures the energy E deposited. The EMCAL has an energy resolution of $8.2\%/\sqrt{E(\text{GeV})} \oplus 1.9\%$ for test beam electrons. Electron identification is performed using the RICH and the EMCAL [14]. The RICH is filled with 1 atm CO₂ radiator and detects on average 10.8 photo-electrons per electron track, while a pion with $p < 4.7$ GeV/c produces no signal. It is required that at least 3 RICH hits are associated with the track and that their hit pattern is consistent with that of an electron track. After these cuts, a clear electron signal is observed as a narrow peak centered at $E/p = 1.0$. We select tracks in the peak as electron candidates. The E/p cut reduces hadron background, and removes conversion electrons created far from the vertex. A hadron deposits only a fraction of its energy in the EMCAL, and the momentum of an off-vertex conversion electron is reconstructed incorrectly. The remaining background, about 10% of the electron candidates, is caused by accidental association of RICH hits with hadron tracks. The level of the background is measured statistically by an event mixing method, and is subtracted from the yield.

The electron acceptance and reconstruction efficiency are determined using a detailed GEANT [15] simulation, which satisfactorily reproduces the detector response. In high multiplicity events, the reconstruction efficiency is reduced due to detector occupancy. This effect is evaluated by embedding simulated electrons into real events. The efficiency loss has no significant p_T dependence for $p_T > 0.4$ GeV/c, and is $27 \pm 4\%$ for the 10% most central collisions and $4 \pm 2\%$ for 60-80% centrality.

Figure 1 shows the p_T distributions of electrons in PHENIX for central (0-10%), minimum bias (0-92%), and peripheral (60-80%) collisions. The centrality selection is provided by a combination of BBC and ZDC signals [16]. Errors in the figure are statistical. The sys-

tematic uncertainty is about 11%. Expected sources of electrons are (1) Dalitz decays of π^0 , η , η' , ω , and ϕ , (2) di-electron decays of ρ , ω , and ϕ , (3) photon conversions, (4) kaon decays ($K^{0,\pm} \rightarrow \pi e\nu$), (5) semi-leptonic decay of charm, and (6) other contributions such as bottom decays and thermal di-leptons. Sources (1)-(4) are considered to be background.

We have calculated the contributions from Dalitz and di-electron decays with a hadron decay generator. PHENIX has measured the p_T distributions of π^\pm in $0.2 < p_T < 2.2$ GeV/c [17] and of π^0 in $1 < p_T < 4$ GeV/c [13]. Since the π^\pm and π^0 data are consistent in the overlapping region, we fit a power law function to the combined data sets to determine the input π^0 spectrum for the decay generator. The p_T distribution of any other hadron h is obtained from the π^0 spectrum by replacing p_T with $\sqrt{p_T^2 + m_h^2 - m_{\pi^0}^2}$. The shapes of the resulting p_T spectra of K^\pm , p , and \bar{p} agree with the PHENIX measurements [17] within 20%. By construction h/π^0 ratios approach constants at high p_T . We assume the following asymptotic ratios to fix the relative normalizations: $\eta/\pi^0 = 0.55$, $\eta'/\pi^0 = 0.25$, $\rho/\pi^0 = \omega/\pi^0 = 1.0$, $\phi/\pi^0 = 0.40$. Except for the ϕ , these ratios are taken from proton beam data of SPS, FNAL, and ISR experiments [18,19]. The η/π^0 ratio is consistent with a measurement in Pb+Pb collisions at the SPS [18]. The ϕ/π^0 ratio is based on the integrated ratio $\phi/h^- \sim 0.02$ in Au+Au collisions at $\sqrt{s_{NN}} = 130$ GeV [21]. We assign to each ratio a conservative systematic uncertainty of 50%.

Photon conversions are evaluated using a combination of the GEANT simulation and the hadron decay generator. Since the p_T spectra of externally converted electrons are almost identical to those from Dalitz decay, a good approximation of the conversion spectra can be made by scaling the Dalitz decay spectra by an appropriate factor, $R_{conv} = \text{Conversion}/\text{Dalitz}$, which is evaluated using the GEANT simulation. The simulation was cross-checked by comparing the relative yield of reconstructed Dalitz pairs and conversion pairs in the simulation and in real data. The simulation shows that R_{conv} has a weak p_T dependence, primarily due to the energy dependence of the pair creation cross section. R_{conv} is parameterized as $(1.9 \pm 0.2) \times (1 - 0.0718 \times p_T^{-0.76})$.

Background from kaon decays is also evaluated using the GEANT simulation, and is found to be negligible.

The upper panel of Fig. 2 shows the ratio of the measured electrons to the calculated background as a function of p_T for minimum bias events. The shaded region is the quadratic sum of the systematic errors in the electron measurement and the uncertainties in the background. The latter includes (1) uncertainties in the normalization and the shape of the input π^0 spectrum, (2) uncertainties in the h/π^0 ratios, and (3) uncertainties in R_{conv} . A significant electron excess above the background is observed for $p_T > 0.6$ GeV/c. Central collisions show a similar ex-

cess. Peripheral collisions do not have sufficient statistics to see a signal in this analysis.

Fractional contributions to the background are shown in the lower panel of Fig. 2. More than 80% of the background is from π^0 decay, directly from the Dalitz decay or indirectly from photon conversion. The π^0 spectrum is well constrained by the PHENIX measurement. The next most important background source is η decay. The 50% uncertainty assigned to the ratio $\eta/\pi^0 = 0.55$ is conservative, since an even larger η/π^0 ratio would imply that η production at high p_T is close to or larger than primary π^0 production. Contributions from all other hadrons combined are only a few percent of the total.

Background-subtracted electron spectra are shown in Fig. 3. The error bars on the data points represent the statistical errors, while the systematic error due to the background subtraction is indicated by brackets. The integrated yield of the electron signal dN_e/dy for $p_T > 0.8$ GeV/c is $0.025 \pm 0.004(\text{stat.}) \pm 0.010(\text{sys.})$ for central collisions and is $0.0079 \pm 0.0006(\text{stat.}) \pm 0.0034(\text{sys.})$ for minimum bias collisions.

Semi-leptonic decay of charmed hadrons is an expected source of the electron signal. We use the event generator PYTHIA [22] to estimate electron spectra from charm decay. We tuned the parameters [24] of PYTHIA such that charm production data at SPS and FNAL [25] and single electron data at the ISR [9–11] are well reproduced. The charm production cross section in pp collisions from this PYTHIA calculation is $\sigma_{c\bar{c}} = 330 \mu\text{b}$ at $\sqrt{s} = 130$ GeV. The electron spectrum in Au+Au collisions is then calculated as $EdN_e/dp^3 = T_{AA} \times Ed\sigma_e/dp^3$, where $Ed\sigma_e/dp^3$ is the electron spectrum from charm decay calculated with PYTHIA, and T_{AA} (listed in Table I) is the nuclear overlap integral calculated from a Glauber model [13]. The calculated electron spectra displayed in Fig. 3 are in reasonable agreement with the data.

Before attributing the entire single electron signal to open charm decays, it is necessary to quantify contributions from other possible sources. An analogous PYTHIA estimate of the bottom decay contribution for central collisions is displayed in Fig. 3. It becomes significant only above the measured p_T range. Expected contributions from J/Ψ and Drell-Yan are found to be negligible. In Pb+Pb collisions at the SPS, direct photons [20] and an enhanced yield of low mass electron pairs [26] have been reported. If these are due to thermal radiation from hot matter, even larger production is expected at RHIC energies, and can contribute to the observed electron signal. Since $\rho \rightarrow e^+e^-$ contributes less than 1% to the calculated background as shown in Fig. 2, and since the dominant source of thermal di-leptons is $\pi + \pi \rightarrow \rho \rightarrow e^+e^-$ [27], a significant contribution from thermal di-leptons is unlikely. There are several predictions for direct photons at RHIC energies [28,29]. The conversion electron spectrum calculated from a prediction in ref. [28] is shown in Fig. 3 for central collisions.

It can contribute 10–20% to the signal, with large theoretical uncertainties.

Neglecting these other possible contributions and assuming that all of the electron signal is from charm, we derive the charm cross section corresponding to the electron data. We fit the charm electron spectrum from PYTHIA to the PHENIX data for $p_T > 0.8$ GeV/c, and obtain the rapidity density $dN_{c\bar{c}}/dy|_{y=0}$ and the total yield $N_{c\bar{c}}$ of open charm. They are then converted to cross sections per NN collision: $d\sigma_{c\bar{c}}/dy = (dN_{c\bar{c}}/dy)/T_{AA}$ and $\sigma_{c\bar{c}} = N_{c\bar{c}}/T_{AA}$. Results are shown in Table I. The systematic error is the quadratic sum of background subtraction (dominant) and dependencies on PYTHIA parameters, parton distribution functions, and fit range. Note that any contributions from neglected sources would reduce the derived charm cross section. If there are no nuclear or medium effects in charm production, the cross section per NN collision should be independent of centrality. The data are consistent with this expectation, but with uncertainties that make any strong conclusion premature.

The single electron signal yield (divided by T_{AA} to give the cross section per NN collision) and the derived charm cross section are compared with single electron data of ISR experiments and charm data of fixed target experiments [25] in Fig. 4. Cross section curves calculated with PYTHIA, which has been tuned to the charm data and the ISR electron data, and a charm cross section curve from a next-to-leading order (NLO) QCD calculation [30] are also shown in the figure. Our data are consistent with both of the calculations within large uncertainties.

In conclusion, we have observed single electrons above the expected background from decays of light hadrons and photon conversion in Au+Au collisions at $\sqrt{s_{NN}} = 130$ GeV. The observed signal is consistent with semi-leptonic decay of charm. The forthcoming high statistics Au+Au data and pp comparison data at full RHIC energy ($\sqrt{s_{NN}} = 200$ GeV) will be useful to clarify the nature of the single electron signal and to better determine heavy-quark production in Au+Au collisions at RHIC.

We thank the staff of the Collider-Accelerator and Physics Departments at BNL for their vital contributions. We acknowledge support from the Department of Energy and NSF (U.S.A.), Monbu-sho and STA (Japan), RAS, RMAE, and RMS (Russia), BMBF, DAAD, and AvH (Germany), VR and KAW (Sweden), MIST and NSERC (Canada), CNPq and FAPESP (Brazil), IN2P3/CNRS (France), DAE and DST (India), KRF and CHEP (Korea), and the US-Israel Binational Science Foundation.

* Deceased

† Not a participating institution.

- [1] J.A. Appel, Ann. Rev. Nucl. Part. Sci. **42**, 367 (1992).
- [2] B. Müller and X.N. Wang, Phys. Rev. Lett. **68**, 2437 (1992).
- [3] Z. Lin and M. Gyulassy, Phys. Rev. Lett. **77**, 1222 (1996).
- [4] Y.L. Dokshitzer and D.E. Kharzeev, Phys. Lett. **B519**, 199 (2001).
- [5] T. Matsui and H. Satz, Phys. Lett. **B178**, 416 (1986).
- [6] M.C. Abreu *et al.*, Phys. Lett. **B447**, 28 (2000).
- [7] R. Vogt *et al.*, Phys. Rev. **D49**, 3345 (1994).
- [8] F. W. Büsser *et al.*, Phys. Lett. **B53**, 212 (1974).
- [9] F. W. Büsser *et al.*, Nucl. Phys. **B113**, 189 (1976).
- [10] P. Perez *et al.*, Phys. Lett. **B112**, 260 (1982).
- [11] M. Basile *et al.*, Nuovo Cimento **A65**, 421 (1981).
- [12] I. Hinchliffe and C. H. Llewellyn Smith, Phys. Lett. **B61**, 472 (1976); M. Bourquin and J.-M. Gaillard, Nucl. Phys. **B114**, 334 (1976).
- [13] K. Adcox *et al.*, Phys. Rev. Lett. **88**, 022301 (2002).
- [14] H. Hamagaki *et al.*, Nucl. Phys. **A698**, 412 (2002).
- [15] GEANT User's Guide, 3.15, CERN Program Library.
- [16] K. Adcox *et al.*, Phys. Rev. Lett. **86**, 3500 (2000).
- [17] K. Adcox *et al.*, nucl-ex/0112006.
- [18] R. Albrecht *et al.*, Phys. Lett. **B361**, 14 (1995); G. Agakichiev *et al.*, Eur. Phys. J. **C4**, 249 (1998) and references therein.
- [19] M. Diakonou *et al.*, Phys. Lett. **B89**, 432 (1980).
- [20] M. M. Aggarwal *et al.*, nucl-ex/0006007; M. M. Aggarwal *et al.*, Phys. Rev. Lett. **85**, 3595 (2000).
- [21] C. Adler *et al.*, to be published.
- [22] T. Sjostrand, Comp. Phys. Commun. **82**, 74 (1994).
- [23] H. L. Lai *et al.*, Eur. Phys. J. **C12**, 375 (2000).
- [24] We used PYTHIA 6.152 with CTEQ5L [23] parton distribution functions. Modified PYTHIA parameters are: PARP(91)=1.5 ($\langle k_T \rangle$), PMAS(4,1)=1.25 (m_c), PARP(31)=3.5 (K factor), MSTP(33)=1, MSTP(32)=4 (Q^2 scale).
- [25] G. A. Alves *et al.*, Phys. Rev. Lett. **77**, 2388 (1996) and references therein.
- [26] G. Agakichiev *et al.*, Phys. Lett. **B422**, 405 (1998).
- [27] R. Rapp, Phys. Rev. **C63**, 054907 (2001).
- [28] J. Alam *et al.*, Phys. Rev. **C63**, 021901 (2001).
- [29] F. D. Steffen and M. H. Thoma, Phys. Lett. **B510**, 98 (2001); D. K. Srivastava, nucl-th/0103023.
- [30] M. Mangano, P. Nason, and G. Ridolfi, Nucl. Phys. **B405**, 507 (1993). Their program **HVQMNR** is used with CTEQ5M [23] parton distribution functions to calculate the charm cross section in Fig. 4.
- [31] The 1.0-1.4 GeV/c point of CCFS is calculated from the e/π ratio in ref. [9] and the pion cross section in B. Alper *et al.*, Nucl. Phys. **B100**, 237 (1975).

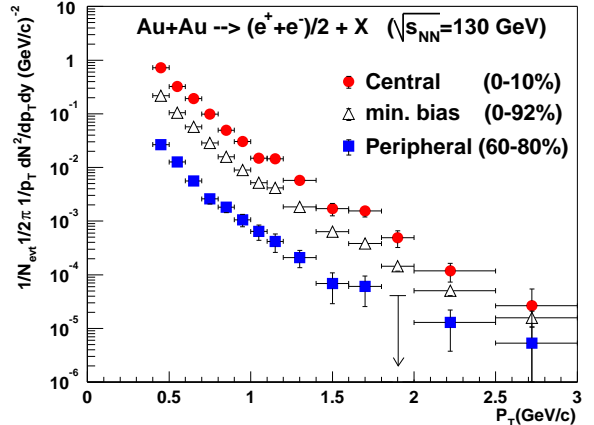


FIG. 1. Transverse momentum spectra of electrons in PHENIX from Au+Au collisions at $\sqrt{s_{NN}}=130$ GeV.

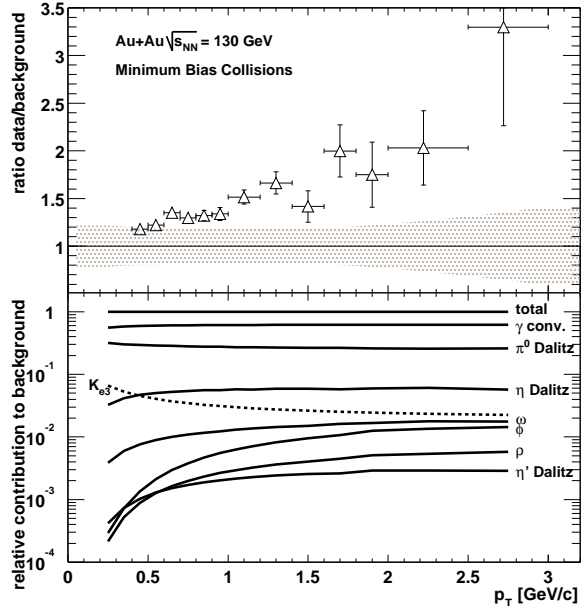


FIG. 2. Ratio of the electron data to the calculated background as a function of p_T in minimum bias collisions (upper panel) and relative contributions to the background from various sources (lower panel). The curves for ω and ϕ show the sum of the Dalitz and the di-electron decay modes.

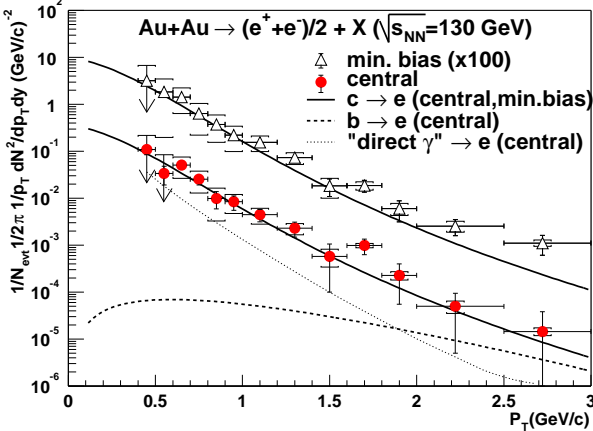


FIG. 3. The background-subtracted electron spectra for minimum bias (0-92%) and central (0-10%) collisions with expected contributions from open charm decays. Also shown, for central collisions only, are the expected contribution from bottom decays (dashed) and the conversion electron spectrum from a direct photon prediction (dotted).

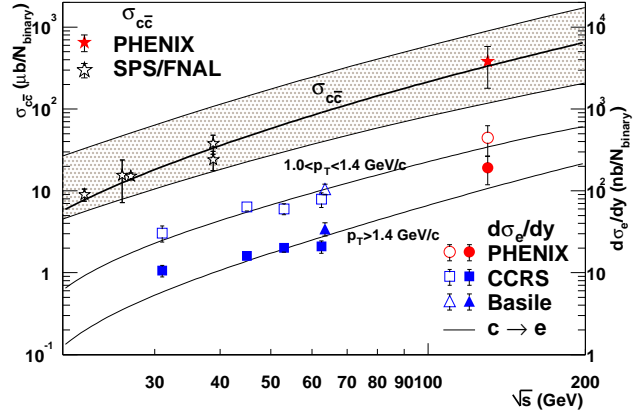


FIG. 4. Single electron cross sections $d\sigma_e/dy|_{y=0}$ of this measurement and ISR experiments [9,11,31] are displayed (bottom of fig., right-hand scale) with charm decay contributions calculated with PYTHIA. Open and filled symbols are for $1.0 < p_T < 1.4$ GeV/c and $p_T > 1.4$ GeV/c, respectively. The derived charm cross section of this measurement is compared with charm cross sections from SPS/FNAL experiments (top of fig., left-hand scale). The thick curve and the shaded band represent the charm cross section in the PYTHIA model and in a NLO pQCD calculation, respectively.

TABLE I. Charm cross section per NN collision derived from the single electron data for central (0-10%) and minimum bias (0-92%) collisions. The first and second errors are statistical and systematic, respectively.

Centrality	$T_{AA}(\text{mb}^{-1})$	$d\sigma_{c\bar{c}}/dy _{y=0}(\mu\text{b})$	$\sigma_{c\bar{c}}(\mu\text{b})$
0-10%	$22.6 \pm 1.6(\text{sys.})$	$97 \pm 13 \pm 49$	$380 \pm 60 \pm 200$
0-92%	$6.2 \pm 0.4(\text{sys.})$	$107 \pm 8 \pm 63$	$420 \pm 33 \pm 250$